Triple Radial Junction Hydrogenated Amorphous Silicon Solar Cells with >2 V Open-Circuit Voltage

Chaoqi Wang, Martin Foldyna, Erik V Johnson, Pere Roca i Cabarrocas

Triple Radial Junction Hydrogenated Amorphous Silicon Solar Cells with > 2 V Open Circuit Voltage

*Chaoqi Wang, Martin Foldyna, Erik V. Johnson, Pere Roca i Cabarrocas**

C. Wang, M. Foldyna, E. V. Johnson, P. Roca i Cabarrocas*

LPICM, CNRS, Ecole Polytechnique, Institut Polytechnique de Paris, Route de Saclay, 91128 Palaiseau, France

E-mail : pere.roca@polytechnique.edu

Keywords: silicon nanowires, hydrogenated amorphous silicon, solar cells, triple junction, high open circuit voltage

Abstract:

When solar cells are used as the photoanode for direct water splitting, the output voltage required typically exceeds that of a single junction photovoltaic device. Towards this application, in this work, triple radial junction silicon nanowire (3RJ SiNW) solar cells are fabricated via a plasma-assisted vapor-liquid-solid method using hydrogenated amorphous silicon (a-Si:H) for all the absorber layers, as well as for the doped ones. A high open circuit voltage (V_{OC}) of 2.05 V, short circuit current density (J_{SC}) of 3.8 mA/cm^2, and power conversion efficiency of 4.4% are obtained for solar cells with areas of 0.03 cm^2 by optimizing the density of SiNWs grown on ZnO:Al/Ag/Corning glass substrates. For lower efficiency devices, however, V_{OC} values as high as 2.2 V are repeatedly achieved. At these higher voltages, large variations in J_{SC} are observed, attributed to small local variations in SiNW density. This work demonstrates for the first time, to our knowledge, the excellent potential of 3D radial junction solar cells for applications requiring high voltages and high surface areas, such as water splitting.

Graphical Abstract:

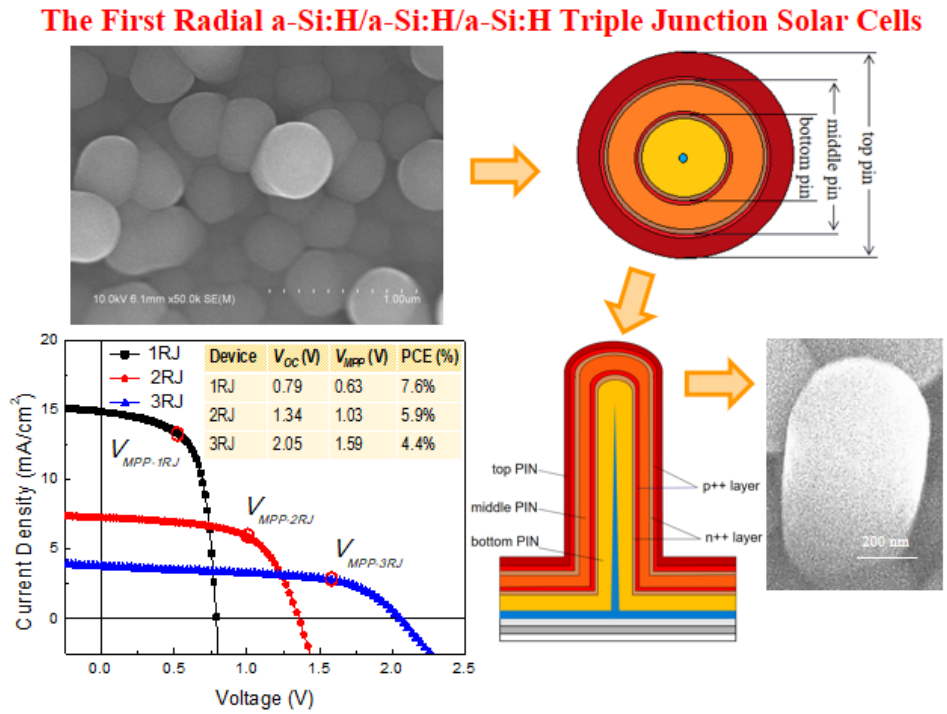

The a-Si:H based triple junction PIN solar cells are built on c-Si nanowires. They deliver 2.05 V open circuit voltage, 3.8 mA/cm^2 current density, 0.57 fill factor, resulting in a 4.4% energy conversion efficiency.

Highlights:

1. a-Si:H/a-Si:H/a-Si:H triple radial junction SiNW solar cells are fabricated.
2. SiNW solar cells with open circuit voltage over 2 V are achieved.
3. SiNWs can improve the contact between ZnO:Al substrate and PIN junction.

1. Introduction

There are many economically viable renewable energy sources available for humankind, but a major challenge is storing the energy [1-4]. Hydrogen is currently being explored as a clean energy vector, and producing hydrogen through water splitting using photovoltaics (PV) is a solution consistent with a low carbon future. Hydrogenated amorphous silicon (a-Si:H), used in a PIN structure, is a promising and robust technology for PV solar cells in terms of silicon abundance, low cost, large areas, and ability to operate in an aqueous environment [5-11]. By combining a-Si:H with lower bandgap materials such as hydrogenated amorphous silicon-germanium or microcrystalline silicon, double (tandem) and triple junction a-Si:H solar cells have been investigated, which yield a higher efficiency due to better utilization of the solar spectrum [12-16]. However, the disordered a-Si:H matrix limits photo-carrier collection and Fermi-level splitting, and leads to conversion efficiencies limited to 12.34% in stabilized 1.4 m^2 tandem micromorph (a-Si:H/μc-Si:H) modules and 16.3% initial efficiency for triple junction devices [17, 18].

However, these structures were optimized for efficiency, and not for the specific application of water splitting. Precisely, a minimum voltage of 1.23 V is required for water splitting, according to thermodynamic calculations [19, 20]. Still, the reaction will proceed infinitely slowly at this voltage, so an even higher voltage is required to drive the reaction, with a greater voltage making the reaction happen faster. In addition to this higher voltage requirement, a technology that is robust, stable, can be produced over large surface areas, and provides a large specific surface area for the catalysis is ideal for this application.

Silicon nanowire (SiNW) solar cells have emerged as an interesting alternative architecture for thin film a-Si:H PV devices [21-24]. In this case, the PIN junction is built on crystalline SiNWs, and forms a radial junction (RJ), which can enhance the light trapping and absorption, allowing for thinner devices. Due to this, a strong built-in electric field is present for better carrier separation and stability against light-induced degradation [6].

Concerning the growth process and structure of SiNW solar cells, there are several

aspects that are ongoing research topics. Firstly, low melting point metal catalysts, such as indium (In), gallium (Ga), bismuth (Bi) and tin (Sn), have been used for SiNW growth in plasma-enhanced chemical vapor deposition (PECVD) [15-18, 25-30]. Recently, mixed metals applied as catalysts for SiNW growth have received increasing attention; for instance, Bi-Sn alloys can provide an n-type doping of SiNWs without the use of toxic dopant gases [24]. As well, a Cu-Sn bimetallic catalyst has been used to grow SiNWs with a metastable hexagonal 2H crystalline structure [31]. Secondly, the growth parameters (RF power, substrate temperature, deposition pressure and doping gases) of SiNWs are also continually studied to further optimize the performance of SiNW solar cells [5]. Finally, the use of low cost and flexible substrates is another promising application for SiNWs. Indeed, single junction SiNW solar cells grown on aluminum foil enable a high power-to-weight performance at low cost. A power conversion efficiency of 5.6% has been recorded even at a bending radius of 5 mm [32].

Combining the RJ concept with a-Si:H multijunctions is another promising research pathway. PIN-PIN tandem a-Si:H solar cells have already been demonstrated in solar mini-modules. Due to their improved stability, they showed a higher end of life aperture efficiency relative to single junction mini-modules [33, 34]. In addition, because a-Si:H/a-Si:H tandem solar cells have lower current density than that of a-Si:H single junction, they can also reduce the resistive losses in the case of a poor conductivity of the transparent conductivity oxide (TCO) substrates [35]. Finally, multijunction solar cells using the same bandgap for the absorber layer are being explored for applications requiring higher voltages, such as for efficient solar to fuel conversion [36].

In this work, triple radial junction (3RJ) SiNW solar cells are demonstrated, with a particular focus on the optimization of the SiNW density to maximize operating voltage. This is done with reference to the voltages needed to achieve water-splitting. The performance of planar a-Si:H solar cells is also studied as a reference case and to understand the limiting factors when optimizing 3RJ solar cells. The 3RJ SiNW solar cells show unique merits as next generation high V_{OC} solar devices, in particular for

water splitting where the operating voltage should be significantly greater than 1.23 V.

2. Experimental Description

2.1 Fabrication of SiNW radial junction solar cells

The first step of the growth of SiNWs is the formation of the catalyst drops (Sn in this work) from which the VLS growth of NWs will occur. In previous works, Fluorine doped SnO_2 (FTO) has been used for SiNW growth, with the Sn droplets formed by a reducing H_2 plasma [37-39]. However, using this approach makes it difficult to control the SiNW density. Therefore, in the current study, the Sn droplets were instead formed from a thin evaporated layer of Sn on top of a 1 inch× 1 inch ZnO:Al/Ag/Corning glass (CG) substrate stack. A 60 nm layer of Ag first was deposited on the CG by RF magnetron sputtering (Alliance Concept) under a RF power of 50 W in 43 sccm Ar for 3 min. Then, 90 nm of ZnO:Al was sputtered with a RF power of 250 W in 30 sccm Ar for 3 min, both at room temperature. The Sn catalyst was deposited on the ZnO:Al/Ag/Cg stack by thermal evaporation in a bell jar chamber. The nominal thicknesses of the Sn catalyst layers are 0.02 nm, 0.08 nm, 0.1 nm, 0.2 nm and 0.8 nm.

The substrates were then loaded into the PECVD chamber. The PECVD tool used in this work is a capacitively-coupled reactor. The top, shower-head electrode is the powered electrode, driven at a frequency of 13.56 MHz, and the bottom, substrate holder electrode is grounded. Both electrodes are heated, and a grounded plasma box is present, surrounding both electrodes. The base pressure of the reactor is below 5×10^{-5} mbar and the working pressure is in the range of 0.1 to 2 mbar. Once base pressure is achieved, the substrates were exposed to a H_2 plasma at 250 ℃ for 2 min in order to reduce the oxide layer formed on top of the evaporated Sn, and obtain Sn droplets. The different thicknesses of Sn give different droplet densities to then be used as catalysts for plasma-assisted vapor-liquid-solid (VLS) growth of SiNWs. The H_2 flow rate, RF power density and chamber pressure were 100 sccm, 5 W and 1.8 mbar, respectively. Afterwards, while the temperature of the substrate holder was increased to 600 ℃, 10 sccm SiH_4, 100 sccm H_2 and 1.5 sccm trimethylboron (1% TMB diluted in H_2) were flowed into chamber. When the substrate reached the nominal temperature of 600 °C, SiNWs were grown for 10 min by igniting a plasma at an RF power of 2 W and a pressure of 1.38 mbar (see Figure 1). After that, the chamber was cooled down to 220 ℃ under an H_2 atmosphere, to be followed by p-type, intrinsic and n-type a-Si:H layer growth by PECVD.

All deposition conditions for single (1RJ), double (2RJ), and triple (3RJ) radial junctions are given in Table 1. For the 1RJ growth, a p-type a-Si:H layer with a dopant gradient was first deposited on SiNWs (Table 1). After the graded p-layer growth, the undoped, i-a-Si:H layer was immediately deposited by closing the TMB flow and allowing growth to continue for 45 min. Then, a graded n-type a-Si:H layer was deposited on the intrinsic a-Si:H layer. This process is depicted in Figure 1.

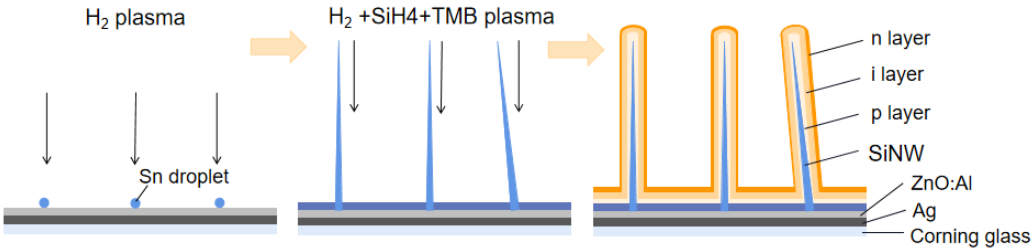

Figure 1. Schematic of the fabrication process of SiNW radial junction solar cells: a) Sn catalyst formation via H_2 plasma treatment; b) p-type SiNWs growth in a mixture of SiH_4, H_2 and TMB; c) The complete pin radial junction solar cell.

Table 1. Parameters for growing SiNW solar cells

Cell	Material	SiH_4 Flow [sccm]	Doping Gas	Doping Gas Flow [sccm]	RF Power [W]	Pressure [mbar]	Time (1J) [min]	Time (2J) [min]	Time (3J) [min]
Bottom	p-a-Si:H	10	1% TMB:H_2	3/2/1	2	0.18	3/1/1	3/1/1	3/1/1
	i-a-Si:H	10	-	-	2	0.16	45	45	32
	n-a-Si:H	10	1% PH_3:H_2	1/2/7	1	0.38	0.7/0.7/2	0.7/0.7/2	0.7/0.7/2
Tunnel	n++ a-Si:H	4	1% PH_3:H_2	10	1	0.28	-	2	2
Junctions	p++ a-Si:H	4	1% TMB:H_2	10	1	0.28	-	2	2
Middle	p-a-Si:H	10	1% TMB:H_2	5	1	0.18	-	-	5
	i-a-Si:H	10	-	-	2	0.16	-	-	16
	n-a-Si:H	10	1% PH_3:H_2	1/2/7	1	0.38	-	-	0.7/0.7/2
Top	p-a-Si:H	10	1% TMB:H_2	5	1	0.18	-	5	5
	i-a-Si:H	10	-	-	2	0.16	-	20	8
	n-a-Si:H	10	1% PH_3:H_2	1/2/7	1	0.38	-	0.7/0.7/2	0.7/0.7/2

For the 2RJ solar cells, after growing the first junction, highly doped n++ and p++ layers were deposited to form a tunnel recombination junction. The conductivities of the n^{++} a-Si:H and p^{++} a-Si:H materials are $\sim 1 \times 10^{-2}$ S/cm and $\sim 3 \times 10^{-5}$ S/cm, respectively.

For the next junction, a p-layer with a constant flow rate of 5 sccm TMB was deposited, and the i-layer and n-layer were deposited as described before (see Table 1).

For the 3RJ solar cells, another n++/p++ junction was deposited after the middle cell. The deposition conditions for the p, i, and n layers were identical to the middle cell, except for the i-layer deposition times (see Table 1). Various steps of the fabrication of 3RJ cells are represented in Figure 2. The side view and top view SEM images of the triple junction are shown in Figure 2 (c) and (d). The final diameter of the triple junction in Figure 2 (d) is around 500 nm. The deposition rate of the intrinsic layer on flat glass substrate was determined to be 0.67 Å/s.

After PECVD, transparent Indium Tin Oxide (ITO) top contact pads were sputtered on the solar cells through a shadow mask. The Ar and O_2 flow rates were 43 and 3 sccm, respectively, using a RF power of 200 W for 7 min at 4.4×10^{-3} mbar and 180℃. The SiNW solar cells were annealed in air at 240℃ for 20 min after ITO sputtering. Small Ag dots are placed on top of ITO pads for a better electrical contact between the ITO and the probe. In Figure 2 (e), the picture shows a 1"×1" sample containing 6 cells of 4 mm diameter (0.13 cm^2) and 15 cells of 2 mm diameter (0.03 cm^2) with ITO top contact. Figure 2(f) shows a SEM image of the triple junction with ITO top contact. The diameter of triple junction with ITO pads in Figure 2(f) is around 600 nm.

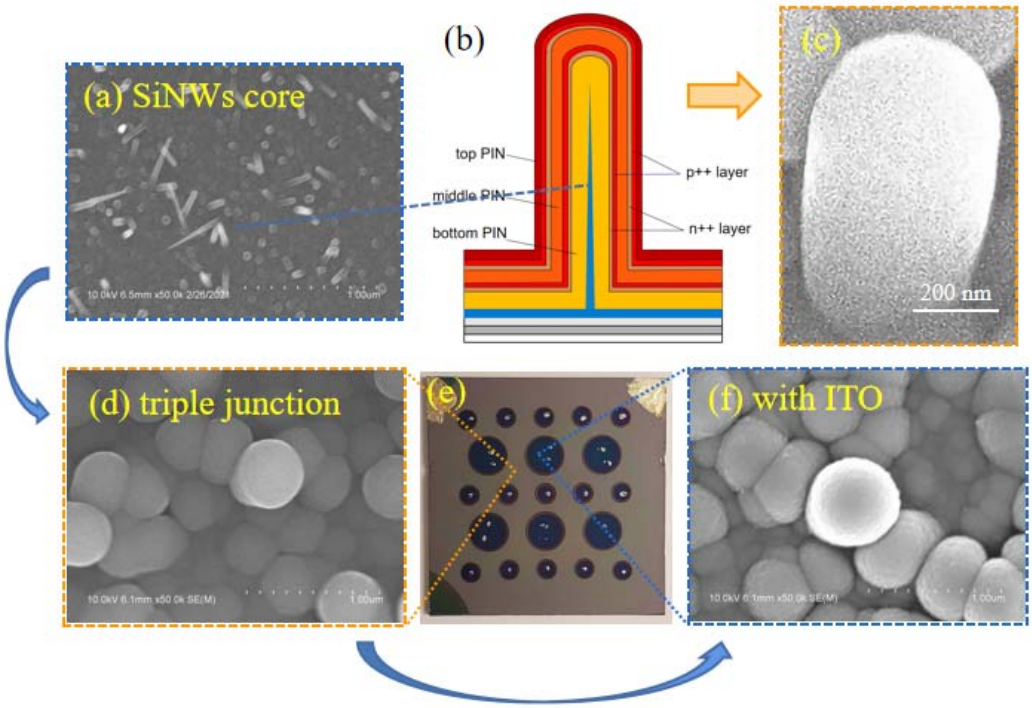

Figure 2. Scanning electron image of SiNW core a) and schematic illustration of the 3RJ solar cell b), triple junction stack around one NW c), triple junction stack of and ensemble of 3RJs without ITO d) photograph of 1" x1" substrate e), 3RJ cells with ITO top contact f).

Planar a-Si:H solar cells were prepared using the same process steps on FTO substrates (MSE Supplies), but without the evaporation of the Sn catalyst nor the p type SiNWs growth.

2.2 Characterization

The current density-voltage (J-V) characteristics of the ~0.03 cm^2 solar cells were measured at room temperature under standard AM1.5G illumination conditions with a power density of 100 mW/cm^2 (Solar Simulator, Newport). These measurements were performed in-house, and were not verified at a third-party measurement laboratory. As mentioned above, before measuring the solar cells, small contacts made from Ag paste were placed by hand on the top of ITO contacts (as shown in Figure 2 e). Due to the manual placement of these contacts, accidental partial shading by the probe, and the

fact that no shadow mask was used during measurement, the J_{SC} of the solar cells can vary. The absolute measured values of J_{SC} have not been confirmed by EQE and should be considered as approximate (±10%). The morphology of solar cells was characterized by scanning electron microscopy (SEM, HITACHI S-4800). The silicon nanowire density was calculated by counting the radial junctions visible in SEM without ITO top contact, as demonstrated in the supplementary material (SI 1).

3. Results and Discussion

3.1 Optimizing SiNW density for triple junction devices

As shown in the work of S. Misra, there is an optimum in the density of single radial junction solar cells of ~2.6×10^8/cm^2 [6]. In that work, it was shown that starting from a planar structure, short circuit current (I_{SC}) increases with NW density due to light trapping, but the reverse dark saturation current (I_0) also increases due to the greater effective surface area. One notes that there are 100's of millions of NWs per square centimeter in such devices, so the increase in effective surface area can be dramatic. The optimum occurs due to the tradeoff between I_{SC} and open circuit voltage (V_{OC}), as approximated by V_{OC} =kTln (I_{SC}/I_0). At yet higher densities, non-uniform radial deposition along the length of the SiNW was also observed, which may play a role too. For 3RJ SiNW solar cells, the total thickness of the stack is obviously greater than that of the single junction. Therefore, the optimum density of SiNWs remains to be determined for 3RJ solar cells.

In Figure 3, SEM images of the SiNW and complete 3RJ a-Si:H solar cells (without ITO top contact) are presented. The density of silicon nanowire solar cells was calculated by counting the radial junctions without sputtered ITO top contact, as shown in the right row of images in Figure 3 (and as demonstrated in supplementary materials SI1). The densities are 1.2×10^8/cm^2, 1.7×10^8/cm^2, 2.2×10^8/cm^2, 3.5×10^8/cm^2 and 4.3×10^8/cm^2. From Figure 3 one can see that the diameter of the silicon nanowire solar cells decreases as their density increases [6-8, 23]. This is expected because the flux of reactive species supplied by the plasma is constant while the total surface of the radial junctions increases with SiNW density.

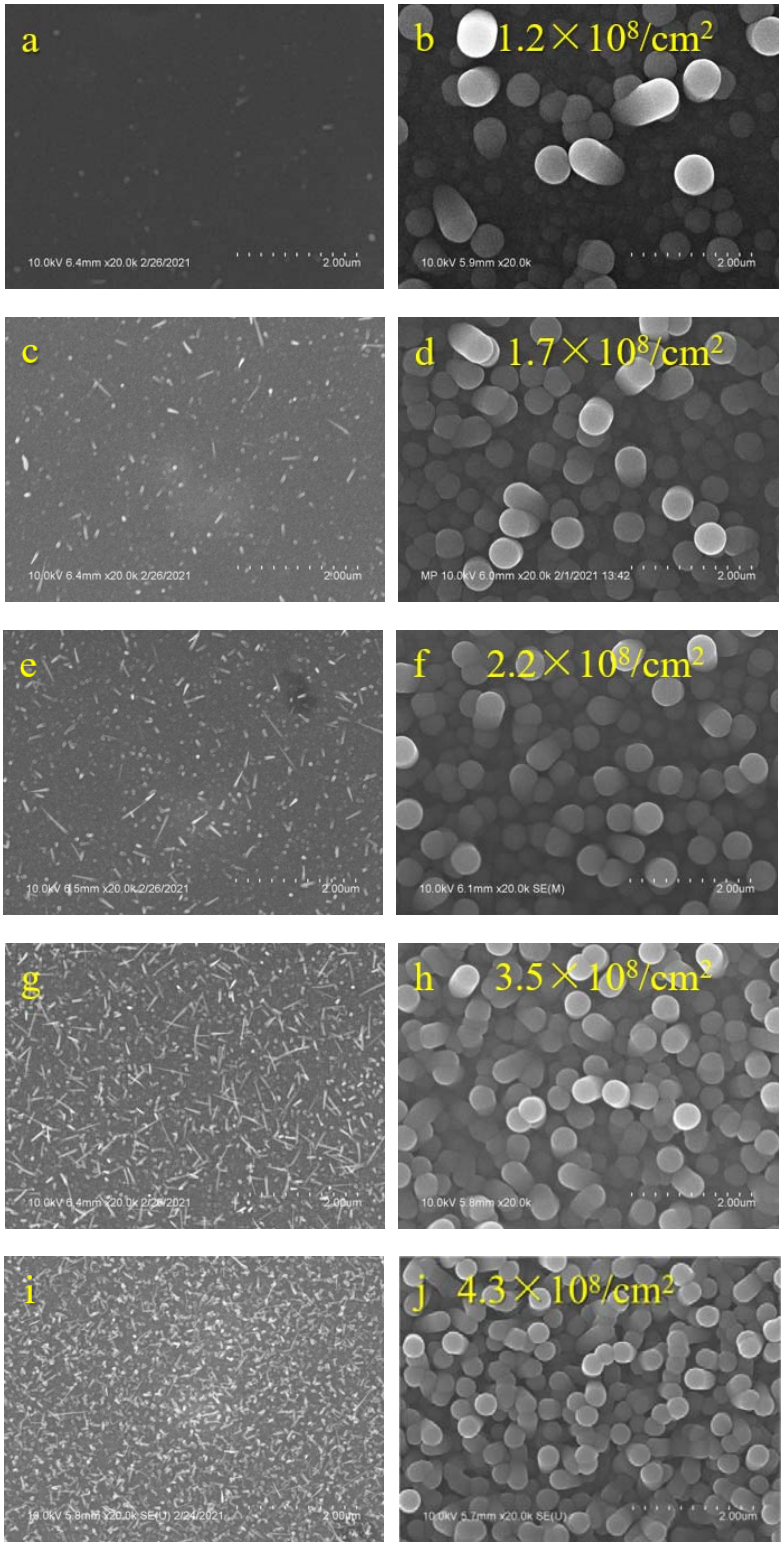

Figure 3. SEM images of SiNWs and 3RJ solar cells. Left row: SiNWs after VLS growth Right row: 3RJ solar cells with densities ranging from 1.2×10^8/cm^2 to 4.3×10^8/cm^2.

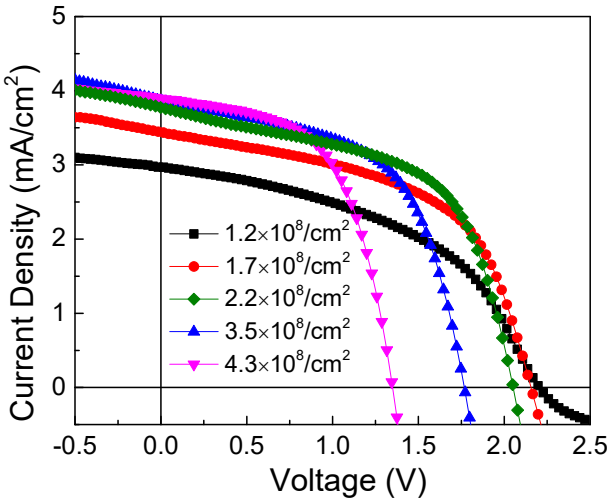

Figure 4. J-V characteristics of 3RJ solar cells with different SiNW densities ranging from 1.2×10^8/cm^2 to 4.3×10^8/cm^2.

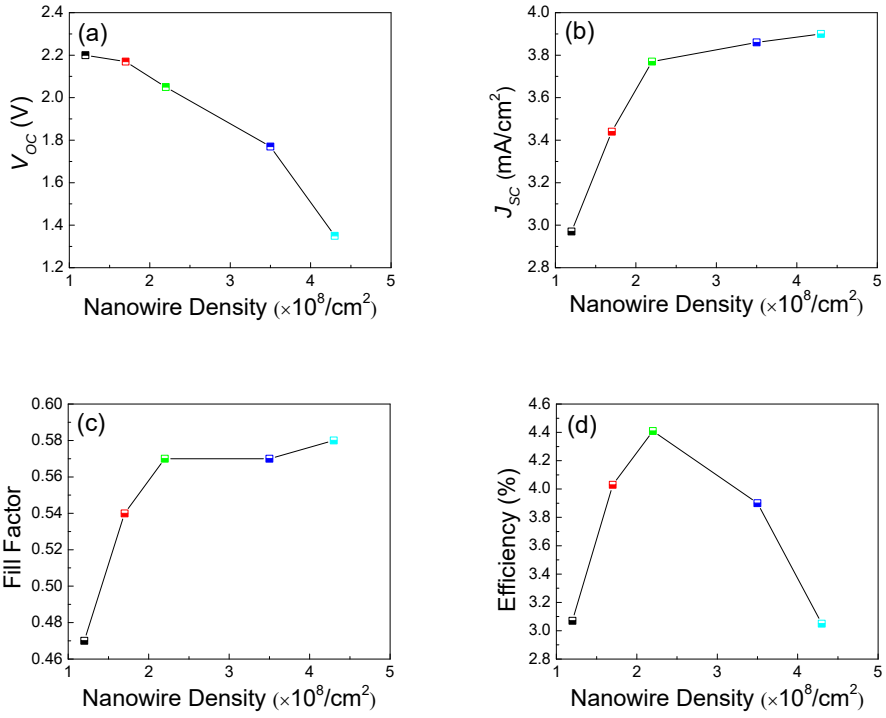

Figure 5. (a)-(d) The open circuit voltage (V_{OC}), the short current density (J_{SC}), fill factor (FF) and power conversion efficiency (η) of a-Si:H 3RJ solar cells as functions of SiNW density.

The J(V) characteristics of 3RJ solar cells with different densities are presented in Figure 4. The open circuit voltage (V_{OC}), short circuit current density (J_{SC}), fill factor (FF) and conversion efficiency (η) of the best 3RJ solar cells are plotted as functions of SiNW densities in Figure 5(a)-(d), respectively.

As expected, Figure 5 (a) shows that V_{OC} decreases as the density of SiNWs increases. At low SiNW density of $1.2\times10^8/cm^2$, a V_{OC} of 2.2 V is obtained but V_{OC} drops to 1.35 V for a density of $4.3\times10^8/cm^2$. As discussed at the start of this section, a higher density of NWs increases the effective surface area of the devices. This increases the dark saturation current, I_0, compared to a planar device. Once this effect is not fully compensated by the increased short circuit current density, I_{SC}, this will lead to a decreased V_{OC} ($V_{OC} = kTln(I_{SC}/I_0)$) [40-43]. Indeed, light trapping is more efficient with increased SiNW density [6, 44, 45]. Figure 5 (b) shows a step increase in J_{SC}, but it flattens out for SiNW densities above 2.2×10^8 cm^{-2} reaching a maximum of 3.9 mA/cm^2 for a density of $4.3\times10^8/cm^2$. Surprisingly, Figure 5(c) shows that the fill factor of 3RJ solar cells increases quickly with SiNW densities from $1.2\times10^8/cm^2$ to $2.2\times10^8/cm^2$. Afterwards, the FF has a slow increase from SiNW density of $2.2\times10^8/cm^2$ to $4.3\times10^8/cm^2$. This is due to poor electrical contact between the absorber layers and the planar areas between NWs, which increases in importance at low NW density. The devices with the lowest density of SiNWs ($1.2\times10^8/cm^2$) display an "S-curve", with a change of inflection around V_{OC}. This behavior is addressed in more detail in SI 2 and 3.

The calculated efficiency of 3RJ solar cells as a function of SiNW density is shown in Figure 5(d), with a clear maximum at $2.2\times10^8/cm^2$ giving the best efficiency of 4.44%. At this point, the J_{SC} has increased to a higher value, but V_{OC} has not yet begun to dramatically decrease.

As expected, the SiNW density corresponding to the best performance is different in single and triple junction. The best density value decreases from $2.6\times10^8/cm^2$ in the case of the SJ [6] to $2.2\times10^8/cm^2$ in the case of the 3RJ. For 3RJ silicon nanowire solar cells, the optimum density is expected to be lower because they have a larger diameter than SJ.

3.2 Top layer thickness and SiNW density effect in high V_{OC}, 3RJ devices

For the devices shown above, a first choice was made that the ratios of the layer thicknesses in the 3J should go as 1:2:4 to approach current matching conditions. However, this choice vastly oversimplifies the optimized choice of layer thicknesses for 3RJ solar cells. To nevertheless analyze the dependence of the device behavior on this ratio, a set of samples have been fabricated, varying the thicknesses of the top layers. As already seen in Figure 5 above, the PV parameters achieved depend very strongly on the value of NW density, particularly around the local efficiency optimum. Therefore, we have chosen devices with similar, elevated values of V_{OC} (2.11 to 2.2 V), as a proxy for local NW density, as this parameter is the hardest to control in this technology.

Two representative J(V) curves of devices with areas of 0.125 cm^2 from each substrate are presented in Figure 6(a). Furthermore, the statistical spread of V_{OC} and J_{SC} for all working 0.125 cm^2 cells on each substrate are presented in Figures 6(b) and 6(c).

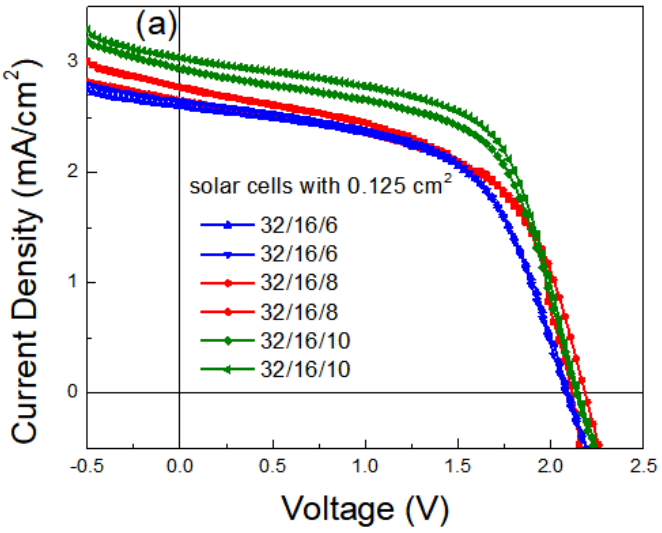

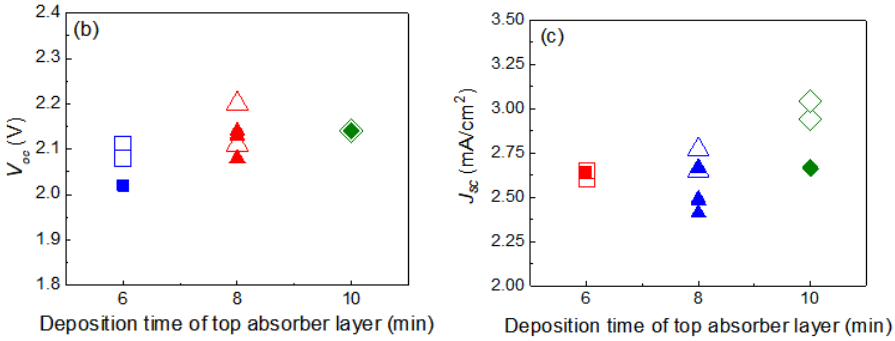

Figure 6. (a) J-V curves for SiNW 3RJ solar cells for three different deposition times (thicknesses) of the top cell. (b) V_{OC} and (c) J_{SC} values of all working cells on substrate, with cells of (a) highlighted as larger, open symbols.

The J-V curves of Figure 6(a) highlight two important facts: firstly, the elevated V_{OC} underlined in this work (targeted towards applications such as water splitting) is shown to be quite robust to variations in top layer thickness. Values above 2V are consistently produced. Secondly, the increasing thickness of the top i-layer seems to increase the overall J_{SC} (and the overall performance, as seen in Figure 6a). As the J_{SC} in such structures is determined by the current-limiting cell [46-48], this indicates that the top-cell is limiting in the present design. One should also note that the ratio of deposition times should not be interpreted as a thickness ratio, as it would be for planar devices. Due to the RJ architecture, under constant plasma conditions, deposition rate will

decrease with time as the SiNW increases in diameter and develops a larger surface area. Furthermore, the spread in values of J_{SC} on a single substrate (Figure 6c) shows difficulty of optimizing such high V_{OC} devices. As one can infer from Figure 5, when targeting high V_{OC} values, one must use lower densities of NWs ($< 2\times10^8/cm^2$), and in this range of densities, the short circuit current density is very sensitive to NW density. In addition, process variations due to ZnO scattering, NW length, ITO contacts, and Ag spot placement will impact J_{SC}, while V_{OC} remains quite stable.

4. Discussion

4.1 Comparing performance of 1J, 2J, 3J solar cells

It is interesting to directly compare the performance of single, double, and triple junction devices made from a single absorber layer material. The J-V characteristics of 1RJ, 2RJ, and 3RJ solar cells are shown in Figure 7, and the associated PV parameters are given in Table 2.

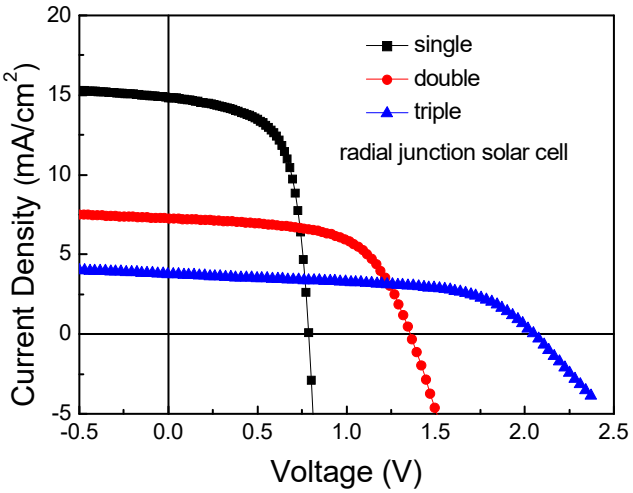

Figure 7. J-V characteristics of radial junction silicon nanowire solar cells with single, double and triple junction.

As shown in Table 1, the V_{OC} values of the 1RJ, 2RJ, and 3RJ SiNW solar cells are 0.79 V, 1.34 V and 2.05 V, respectively. According to the single diode model

describing a solar cell, one can use the formula V_{OC}= nkT ln(J_{SC}/J_0) to describe the tendency of V_{OC} as a function of illumination (approximated by J_{SC}). All else remaining equal, if the current density becomes lower, the V_{OC} will also decrease. For example, using this calculation, the expected V_{OC} for a double junction based on a single junction with 0.79V would be between 1.54 and 1.51V depending on the value of n, ignoring voltage losses in the tunnel junction [49]. For a triple junction, the expected values would be between 2.11V and 2.28V, so in fact, the voltage in the triple junction is very close to the maximum achievable value if we assume constant values of J_0 for both devices.

The J_{SC} values compared to the expected maximum are not as impressive for the triple junction. The 14.8 mA/cm^2 of the single junction could be divided between two junctions giving 7.4 mA/cm^2 each (actually 7.1 mA/cm^2) or three junctions, giving 4.9 mA/cm^2 (actually 3.8 mA/cm^2). For the triple junction, some optical management is obviously still necessary to improve absolute efficiency, such as optimizing all layer thicknesses and using n-type hydrogenated microcrystalline silicon oxide (μc-SiO_x:H) as the top-most doped layer [50].

Table 2. V_{OC}, Jsc, FF and power conversion efficiency (PCE) of single, double and triple junction SiNW solar cells.

Device	V_{OC} (V)	V_{MPP} (V)	J_{SC} (mA/cm^2)	FF	PCE (%)
1RJ	0.79	0.63	14.8	0.65	7.6%
2RJ	1.34	1.03	7.1	0.62	5.9%
3RJ	2.05	1.59	3.8	0.57	4.4%

One last point to note in Table 1 is that for the triple junction SiNW solar cells, the voltage at maximum power (V_{MPP}) is sufficiently high to drive unassisted water splitting; 1.23 V is the minimum voltage required for water splitting, plus an overvoltage to increase the rate, depending on the catalysts used [19, 20]. This underlines the interest in such devices for this application, as such 3RJ devices can directly supply such a voltage.

5. Conclusion

With the goal of an elevated operating voltage suitable for water splitting, an a-Si:H based silicon nanowire triple radial junction (SiNW 3RJ) solar cell has been successfully fabricated using a one-pump-down plasma-assisted VLS method. The SiNW solar cell is grown by using a combination of ZnO:Al and evaporated Sn as a substrate and catalyst. The SiNW 3RJ solar cell performance depends strongly on nanowire density. When optimizing for efficiency, a nanowire density of $2.2\times10^{8}/cm^{2}$ leads to a V_{OC} up to 2.05 V, J_{SC} of 3.8 mA/cm^{2}, FF of 0.57 and an efficiency of 4.4%. Higher values of V_{OC} up to 2.2 V are achieved, but at the cost of a greater variability in J_{SC} due to the random nature of SiNW growth.

Acknowledgements

This work was supported by the China Scholarship Council.

Supporting Information

Supporting Information is available from the Wiley Online Library or from the author.

Conflict of Interest

The authors declare no conflict of interest.

References

[1] B. Tian, T.J. Kempa, C. M. Lieber, *Chem. Soc. Rev.* **2009**, 38, 16.

[2] K. Q. Peng, S. T. Lee, *Adv. Mater.* **2011**, 23, 3, 198.

[3] E. C. Garnett, M.L. Brongersma, Y. Cui, M.D *McGehee Res,* **2011,** 41, 269.

[4] M.A. Green, *Prog. Photovolt.: Res. Appl.* **2001**, 9, 123..

[5] S. Misra, L. Yu, W. Chen, M. Foldyna, P. Roca i Cabarrocas, *J. Phys. D: Appl. Phys.* **2014**, 47, 393001.

[6] S. Misra, L. Yu, M. Foldyna, P. Roca i Cabarrocas, *Sol. Energy Mater. Sol. Cells.* **2013**, 118, 90.

[7] L. Yu, F. Fortuna, B. O'Donnell, T. Jeon, M. Foldyna, G. Picardi, P. Roca i Cabarrocas, *Nano Let.* **2012**, 12, 4153.

[8] L. Yu, B. O'Donnell, M. Foldyna, P. Roca i Cabarrocas, *Nanotechnology.* **2012**, 23, 194001.

[9] S. Wagner, *Phys. Status Solidi A.* **2010,** 207, 501.

[10] P. Krogstrup, H.I. Jørgensen, M. Heiss, O. Demichel, V.J. Holm, M. Aagesen, J. Nygard, A. Fontcuberta i Morral, *Nat. Photonics.* **2013**, 7, 306.

[11] J. A. Hamel，K. Sung，T. D. Jarvi，A. J. Esswein，J. J. H. Pijpers，S. Y. Reece，D. G. Nocera, *Science.* **2012**, 334, 645.

[12] S. Zhang, T Zhang, Z. Liu, J. Wang, L. Yu, J. Xu, K. Chen, P. Roca i Cabarrocas, *Nano Energy.* **2021**, 86, 1061121.

[13] F. Meillaud, A.Shah, C.Droz, E.Vallat-Sauvain, C. Miazz, *Sol. Energy Mater. Sol. Cells.* **2006**, 90, 2592.

[14] S. Okamoto, E. Maruyama, A. Terakawa, W. Shinohara, S. Nakano, Y. Hishikawa, K. Wakisaka, S. Kiyama, *Sol. Energy Mater. Sol. Cells.* **2001**, 66, 85.

[15] Q. Fan, C. Chen, X. Liao, X. Xiang, S. Zhang, W. Ingler, N. Adiga, Z. Hu, X. Cao, W. Du, X. Deng, *Sol. Energy Mater. Sol. Cells.* **2010**, 94, 1300.

[16] L. Bai, B. Liu, J. Fan, D. Zhang, C. Wei, J. Sun, Y. Zhao, X. Zhang, *J. Power Sources.* **2014**, 266, 138.

[17] J.S. Cashmore, M. Apolloni, A. Braga, O. Caglar, V. Cervetto, Y Fenner, S. Goldbach-Aschemann, C. Goury, J. E. Hötzel, T. Iwahashi, J. Kalas, M. Kitamura, M.

Klindworth, M. Kupich, G. F. Leu, J. Lin, M. H. Lindic, P. A. Losio, T. Mates, D. Matsunaga, B. Mereu, X. V. Nguyen, I. Psimoulis, S. Ristau, T. Roschek, A. Salabas, E. L. Salabas and I. Sinicco, *Prog. Photovolt.: Res. Appl.* **2015**, 23, 1441.

[18] B. Yan, G. Yue, L. Sivec, J. Yang, S. Guha, C. Jiang, *Appl. Phys. Lett.* **2011**, 99, 113512.

[19] C. Lamy, Pierre Millet *J. of Power Sources.* **2020**, 447, 227350.

[20] I. Holmes-Gentle and K. Hellgardt, *Sci. Rep.* **2018**, 8, 12807.

[21] L. Yu, S. Misra, J. Wang, S. Qian, M. Foldyna, J. Xu, Y. Shi, E. Johnson, P. Roca i Cabarrocas, *Sci. Rep.* **2014**, 4, 4375.

[22] J. Cho, B. O'Donnell, L. Yu, K.H. Kim, I. Ngo, P. Roca i Cabarrocas, *Prog. Photovolt.: Res. Appl.* **2013**, 21, 77.

[23] L. Yu, L. Rigutti, M. Tchernycheva, S. Misra, M. Foldyna, G. Picardi, P. Roca. i Cabarrocas, *Nanotechnology*. **2013**, 24, 275401.

[24] Z Yu, J Lu, S Qian, S Misra, L Yu, J Xu, L Xu, J Wang, Y Shi, K Chen, P. Roca i Cabarrocas, *Appl. Phys. Lett.* **2015**, 107, 163105.

[25] H. Zhang, Y. Lei, Q. Zhu, T. Qing, T. Zhang, W. Tian, M. Lange, M. Jiang, C. Han, J. Li, D. Koelle, R. Kleiner, W. Xu, Y. Wang, L. Yu, H. Wang, P. Wu, *ACS Nano* **2019**,13, 10359.

[26] T. Zhang, J. Wang, L. Yu, J. Xu, P. Roca i Cabarrocas, *Nanotechnology* **2019**, 30, 302001.

[27] L. Yu, B. O'Donnell, P.J. Alet, P. Roca i Cabarrocas, *Sol. Energy Mater. Sol. Cells.* **2010**, 94, 1855.

[28] L. Yu, B. O'Donnell, P.J. Alet, S. Conesa-Boj, F. Peiró, J. Arbiol, P. Roca i Cabarrocas, *Nanotechnology.* **2009**, 20, 225604.

[29] L. Yu, F. Fortuna, B. O'Donnell, G. Patriache, P. Roca i Cabarrocas, *Appl. Phys. Lett.* **2011**, 98, 123113.

[30] I. Zardo, L. Yu, S. Conesa-Boj, S. Estrade, P.J. Alet, J. Rössler, M. Frimmer, P. Roca i Cabarrocas, F. Peiró, J. Arbiol, J.R. Morante, A. Fontcuberta i Morral, *Nanotechnology* **2009**, 20, 155602.

[31] W. Wang, E. Ngo, I. Florea, M. Foldyna, P. Roca i Cabarrocas, J. Maurice, *ACS*

Omega **2021**, 40, 26381.

[32] X. Sun, T. Zhang, J. Wang, F. Yang, L. Xu, J. Xu, Y. Shi, K. Chen, P. Roca i Cabarrocasc, L. Yu, *Nano Energy.* **2018**, 54, 83.

[33] H. Joseph J (RCA Corporation), *US. 4272641*, **1981**. .

[34] Y. Hamakawa, W. Ma, H. Okamoto, *MRS Bulletin.* **1993**, 18, 38.

[35] Bubenzer A,Lechner P, Schade H, Rübel H, *Sol. Energy Mater. Sol. Cells.* **1994**, 34, 347.

[36] U. Félix, S. Vladimir, B. Jan-Philipp, R. Uwe, Z. Jürgen, K. Bernhard, J. Wolfram, F Friedhelm, *Sol. Energy Mater. Sol. Cells.* **2015**, 140, 275.

[37] M. Al-Ghzaiwat, M. Foldyna, T. Fuyuki, W. Chen, E. Johnson, J. Meot, P. Roca i Cabarrocas, *Sci. Rep.*,**2018**, 8, 1.

[38] M. Al-Ghzaiwat, A. Foti, A. Nuesslein, L. Halagacka, J. Meot, A. Labouret, R. Ossikovski, P. Roca i Cabarrocas, M. Foldyna, *Phys. Status Solidi RRL-Rapid Res. Lett.* **2019**, 13, 1800402.

[39] S. Hamma, P. Roca i Cabarrocas, *Sol. Energy Mater. Sol. Cells.* **2001**, 69, 217.

[40] J. Oh, H. Yuan, H. M. Branz, *Nat. Nanotechnology.* **2012**, 7, 743.

[41] Y. Dan, K. Seo, K. Takei, J. H. Meza, A. Javey, K. B. Crozier, *Nano Lett.* **2011**, 11, 6, 2527.

[42] A. Gudovskikh, D. Kudryashov, A. Baranov, A. Uvarov, I. Morozov, A. Maksimova, E. Vyacheslavova, D. Kirilenko,A. Mozharov, *Phys. Status Solidi A.* **2021,** 218, 22, 501.

[43] M. Gharghi, E. Fathi, B. Kante, S. Sivoththaman, X. Zhang, *Nano Let.* **2012**, 12, 12, 6278.

[44] Y. Cao, Z. Ge, X. Jiang, J. Xu, L. Xu, W. Li, L. Yu, K. Chen, *Part. Part. Syst. Charact.* **2016**, 33, 1, 38.

[45] S. Shiu, S. Lin, S. Hung, C. Lin, *Appl. Surf. Sci.* **2011**, 257, 6, 1829.

[46] E. Köhnen, M. Jošt, A. B. Morales-Vilches, P. Tockhorn, A. Al-Ashouri, B. Macco, L. Kegelmann, L. Korte, B. Rech, R. Schlatmann, B. Stannowski, S. Albrecht, *Sustainable Energy Fuels.* **2019**, 3, 8, 1995.

[47] M. Bonnet-Eymard, M. Boccard, G. Bugnon, F. Sculati-Meillaud, M. Despeisse, C. Ballif, *Sol. Energy Mater. Sol. Cells.* **2013**, 117, 120.

[48] C. Ulbrich, C. Zahren, A. Gerber, B. Blank, T. Merdzhanova, A. Gordijn, U. Rau, *Int. J. Photoenergy.* **2013**, 2013, 1.

[49] W. Yao, .Zeng, W. Peng , S. Liu, X. Xie, C. Wang, X. Liao. *Chin. Phys. B.* **2011**, 20, 7, 078402.

[50] L. Dai, M. Foldyna, A. José, I. Maurin, J. Kleider, T. Gacoin, P. Roca i Cabarrocas, *Phys. Status Solidi A.* **2021**, 218, 17, 2100231.